



Microstructure characterization of as-fabricated and 475 °C annealed U–7 wt.% Mo dispersion fuel in Al–Si alloy matrix

Bo Yao^{a,*}, Emmanuel Perez^a, Dennis D. Keiser Jr.^b, Jan-Fong Jue^b, Curtis R. Clark^b, Nicolas Woolstenhulme^b, Yongho Sohn^a

^a Advanced Materials Processing and Analysis Center and Department of Mechanical, Materials, and Aerospace Engineering, University of Central Florida, Orlando, FL 32816, United States

^b Nuclear Fuels and Materials Division, Idaho National Laboratory, P. O. Box 1625, Idaho Falls, ID 83415, United States

ARTICLE INFO

Article history:

Received 16 March 2011

Received in revised form 11 July 2011

Accepted 16 July 2011

Available online 22 July 2011

Keywords:

Nuclear fuels

U(Mo)

Interface

Diffusion reaction

TEM

ABSTRACT

High-density uranium (U) alloys with an increased concentration of U are being examined for the development of research and test reactors with low enriched metallic fuels. The U–Mo fuel alloy dispersed in Al–Si alloy has attracted particular interest for this application. This paper reports our detailed characterization results of as-fabricated and annealed (475 °C for 4 h) U–Mo dispersion fuels in Al–Si matrix with a Si concentration of 2 and 5 wt.%, named as “As2Si”, “As5Si”, “An2Si”, “An5Si” accordingly. Techniques employed for the characterization include scanning electron microscopy and transmission electron microscopy with specimen prepared by focused ion beam in situ lift-out. Fuel plates with Al–5 wt.% Si matrix consistently yielded thicker interaction layers developed between U–Mo particles and Al–Si matrix, than those with Al–2 wt.% Si matrix, given the same processing parameters. A single layer of interaction zone was observed in as-fabricated samples (i.e., “As2Si”, “As5Si”), and this layer mainly consisted of $U_3Si_3Al_2$ phase. The annealed samples contained a two-layered interaction zone, with a Si-rich layer near the U–Mo side, and an Al-rich layer near the Al–Si matrix side. The U_3Si_5 appeared as the main phase in the Si-rich layer in “An2Si” sample, while both U_3Si_5 and $U_3Si_3Al_2$ were identified in sample “An5Si”. The Al-rich layer in sample “An2Si” was amorphous, whereas that in sample “An5Si” mostly consisted of crystalline $U(Al,Si)_3$, along with a small fraction of $U(Al,Si)_4$ and $U_6Mo_4Al_{43}$ phases. The influence of Si on the diffusion and reaction in the development of interaction layers in U(Mo)/Al(Si) is discussed in the light of growth-controlling mechanisms and irradiation performance.

© 2011 Elsevier B.V. All rights reserved.

1. Introduction

High-density uranium (U) alloys with an increased concentration of U are being examined for the development of research and test reactors with metallic fuel that consists of low enriched U ($^{235}U < 20$ at.%) [1]. To that end, U–Mo dispersion fuel in Al–alloy matrix has gained interests [2,3] as it can provide U density up to 8.5 gU/cm^3 [4]. One key challenge in application of U–Mo dispersion fuels in Al–alloy matrix is the development of undesirable interaction layer between the U–Mo alloy particles and Al–alloy matrix during fabrication (i.e., thermo-mechanical) process and/or under irradiation [4–8]. This interaction layer may be responsible for poor irradiation performance of fuels due to the formation of large voids

and pillowing [5,6] in the interaction layer [4]. As indicated by a recent transmission electron microscopy (TEM) study on irradiated U–7 wt.% Mo dispersion fuels [9], a superlattice of fission gas bubble was formed in U(Mo), which was found to be fully coherent with the U(Mo) host lattice. Unfortunately, some glassy interaction layer cannot support the bubble lattice, which consequently causes the bubbles to coalesce and lead to the development of large voids. The pillowing in the interaction zone was caused by the loss of the cladding–fuel bond over a substantial portion of area and the high pressure of fission gas in the interaction region [10]. Additionally, poor thermal performance of the interaction layer (e.g., a large mismatch of the thermal expansion coefficients between interaction products and matrix) may induce a significantly high thermal stress, which can also induce a de-bonding failure at the interface.

A great improvement in irradiation performance was achieved when a small amount of Si (typically less than 10 wt.%) was added into the Al-matrix [11–14]. Simulation and experimental studies have been conducted to understand the role of Si. For example, atomistic modeling [15–17] based on first principle calculations and Monte Carlo simulations suggest that Si is energetically

* Corresponding author at: Suite 304, Materials Characterization Facility (MCF), Advanced Materials Processing and Analysis Center (AMPAC), University of Central Florida, 12443 Research Parkway, Orlando, FL 32826, United States.
Tel.: +1 407 749 8235; fax: +1 407 882 1502.

E-mail address: bo555252@gmail.com (B. Yao).

favorable to diffuse into U, and forms the U–Si compounds at the interface, which are more stable than U–Al products. Experimental characterizations also revealed that the addition of Si can significantly reduce the rate of diffusion and/or reaction [18–32]. Development of a thinner interaction layer enriched with Si has been commonly reported [18–32].

The irradiation behavior of U–Mo dispersion fuels in Al–Si matrix can be strongly influenced by specific phases in the interaction layers that are formed when samples are exposed to high temperature during fabrication process (e.g., hot-rolling, annealing, etc.). For example, presence of phases with a poor irradiation stability, such as $U(Al,Si)_4$ and $U_6Mo_4Al_{43}$, may induce premature failure. Previous characterization of post-irradiation examination of U–7 wt.% Mo dispersion fuel reported that the interaction phase with a composition near 80 at.% Al near Al matrix side has been linked to poor fuel performance [4], and this phase was surmised to be $U_6Mo_4Al_{43}$ and UAl_4 at first. In a follow-up study of U–Mo/Al diffusion couples, the appearance of $U_6Mo_4Al_{43}$ near Al matrix side has been identified [7]. Furthermore, ion irradiation studies [33] performed on alloys that contain $U_6Mo_4Al_{43}$ demonstrated poor irradiation performance defined by formation of amorphous at low radiation doses and the development of large fission gas bubbles. Deleterious performance of UAl_4 phase under irradiation has also been commonly agreed upon [34]. Therefore a better understanding on the phase formation and evolution in the interaction zone between U–Mo dispersion fuels and Al–alloy matrix is of great importance.

Earlier studies have suggested the presence of $U(Al,Si)_3$ [20,24] and U_3Si_5 phases [25] in the interaction layer. Recent studies suggest that there may be many other phases including UMo_2Al_{20} [27,28], $U_6Mo_4Al_{43}$ [26,28,31,32], $U(Si,Al)_2$ [30], $(U,Mo)_{0.9}(Al,Si)_4$ [30], $U_3Si_3Al_2$ [31,32], and $USi_{1.88}$ [31,32]. The discrepancy is partially due to the variation in composition, processing routes of the fuel system and, for the case of solid-to-solid diffusion couples, experimental technique. Furthermore, various analytical techniques with different capabilities and resolution limits for the phase identification may also be responsible for the inconsistency.

So far, majority studies have been focused on relatively thick interaction layers developed between U–Mo fuel and Al–alloy matrix, most probably for the convenience of experimental processing (e.g., bulk sample diffusion couples) and characterization. A clear understanding on the formation of interaction layer, and its behavior under irradiation, starts with a detailed characterization of the *initial* (e.g., *starting*) microstructure that influences further microstructural development. Previously, we reported characterization results of U–Mo dispersion fuels with AA6061 cladding exposed to high temperature of 500 °C [32]. Fabrication of dispersion fuels resulted in a substantial U–Mo/Al interaction, which may be related to a poor irradiation performance. Presence of Si in the interaction layer was qualitatively related to reduce the growth rate of the interaction layer.

In this study, the soft cladding AA5052 was employed for the fabrication at 425 °C, to simulate the performance of fuel plate with softer cladding alloys such as AG3NBE and AlFeNi. For these soft cladding alloys, the elevated temperature of 500 °C or higher, typically used for fabrication of fuel plates with AA6061 cladding, is considered too high [34]. Furthermore, a reduced temperature is helpful to minimize the decomposition of γ -U(Mo) and the formation of $U_6Mo_4Al_{43}$ phase [26,28,34]. This study examined the initial microstructure of fuel plates after fabrication at 425 °C and the microstructural evolution after further thermal annealing at 475 °C. An additional annealing is conducted to enhance the Si diffusion towards the U(Mo)–Al(Si) interface, and form a stable Si-accumulated layer. Phase constituents, thickness, and composition in the pre-irradiated interaction zone are important to the irradiation performance of the fuels [34]. The as-fabricated and thermally

Table 1
Size and distribution of Al powders.

Sieve size (μm)	(%)
>150 μm (100 mesh)	0
>75 μm (200 mesh)	3.6
>45 μm (325 mesh)	12.8
<45 μm (325 mesh)	83.5

Table 2
Composition of Al–Si powder mixtures.

Nominal composition (wt.%)	Measured Si (wt.%)	Measured Fe (wt.%)
Al–2Si	1.98	0.20
Al–5Si	4.82	0.18

Table 3
Fuel plate rolling schedule.

Pass	Soak before pass (min)	Thickness in (cm)	Thickness out (cm)	% Reduction	Reduction (X:1)
1	30	0.95	0.67	30	1.4
2	10	0.67	0.50	25	1.9
3	10	0.50	0.38	25	2.5
4	10	0.38	0.30	20	3.2
5	5	0.30	0.24	20	4
6	5	0.24	0.19	20	5
7	5	0.19	0.16	17	6
8	5	0.16	0.16	0	6

annealed (at 475 °C for 4 h) U–7 wt.% Mo fuels were dispersed in Al matrix with 2 wt.% and 5 wt.% Si. Techniques employed for the characterization include scanning electron microscopy (SEM), focused ion beam (FIB) with in situ lift-out (INLO) technique, and TEM. The phase development and its potential effect on the overall irradiation performance are further discussed.

2. Experimental procedures

The samples examined in this study were fabricated at a temperature of 425 °C using standard fuel plate fabrication steps [31] and a relatively soft cladding (i.e., AA5052). DU–7Mo alloy pins were first fabricated using arc melting and gravity casting. These pins were made into powders using the rotating electrode process. High-purity Si (99.999% Si) and Al (99.5% Al, 0.12% Fe, 0.15% Si) powders were mixed in the various ratios for 30 min in a Turbula Mixer, and then vacuum degassed in a tube furnace. The Si powders were all less than 45 μm (325 mesh) in size, and the available information on the Al powder size distribution is reported in Table 1. Results of chemical analysis of the final Al and Si powder mixtures are reported in Table 2.

Powder compacts that could be used to produce 8 gU/cm³ fuel plates were made in a hardened tool steel die that was designed to make plates at 6:1 rolling reduction. The cladding material used for fuel plate fabrication was AA5052, with a nominal composition of (95.7–97.7)Al–(2.20–2.80)Mg–(0.15–0.35)Cr with less than 0.10, 0.40, 0.10, 0.25, and 0.10 wt.% Cu, Fe, Mn, Si, and Zn, respectively. Rolling of fuel plates to a final thickness of around 1.5 mm was performed by following the schedule listed in Table 3. Small samples (~0.76 cm × 2.54 cm) were sectioned from each plate to be used in annealing experiments. During the rolling, samples were exposed to a temperature of 425 °C for approximately 80 min. In this study, the as-rolled samples are considered as “as-fabricated” and designated as “As2Si” and “As5Si” for fuel plates in Al matrix containing 2 wt.% and 5 wt.% Si, respectively. To understand the microstructural and phase evolution of the interaction layers, the as-fabricated samples (i.e., after the rolling process) were further annealed at 475 °C for 4 h. These annealed samples are labeled as “An2Si” and “An5Si” accordingly. Table 4 lists the fuel plate samples examined in this study.

Table 4
U–7 wt.% Mo dispersion plates in Al–Si alloy matrix characterized in this study.

Sample ID	Al matrix	U(Mo) powders	Processing condition
As2Si	Al–2 wt.% Si	U–7 wt.% Mo	As-fabricated (after hot-rolling)
As5Si	Al–5 wt.% Si		
An2Si	Al–2 wt.% Si		Annealed at 475 °C for 4 h
An5Si	Al–5 wt.% Si		

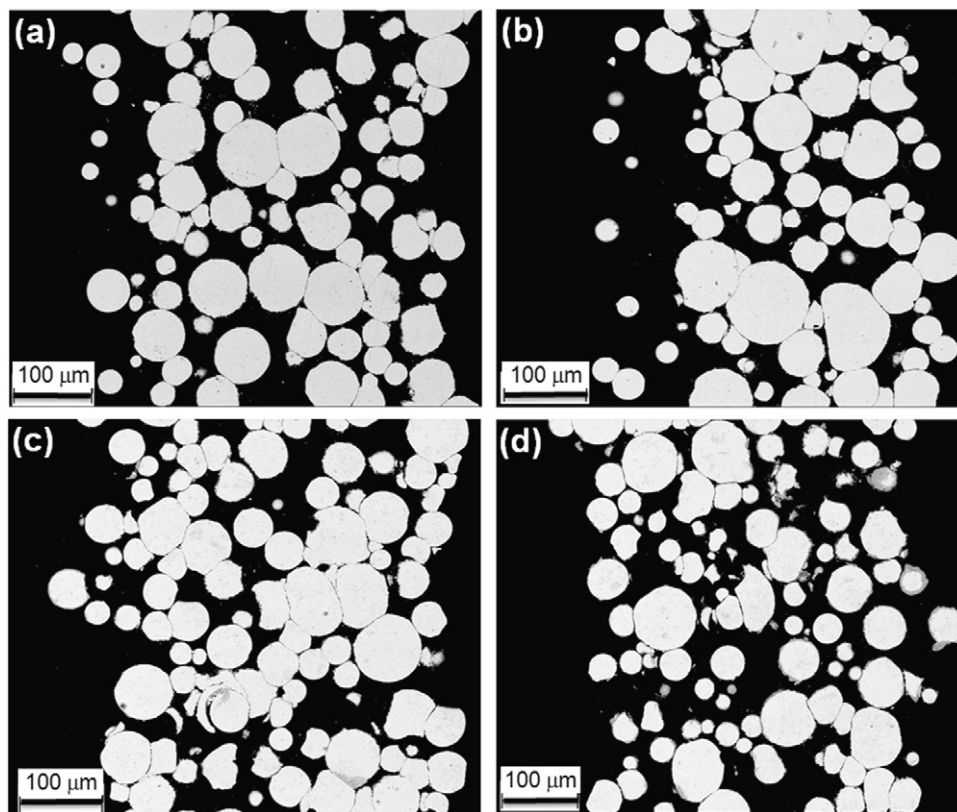


Fig. 1. Back-scattered SEM micrographs providing an overview of U(Mo) dispersion fuels (appeared as bright particles) in Al(Si) matrix (dark background) of samples (a) “As2Si”, (b) “As5Si”, (c) “An2Si”, and (d) “An5Si”.

Cross-sections were prepared from the fuel plates, mounted in epoxy, and then polished for microstructural characterization. SEM was carried out by using a ZeissTM Ultra-55 field emission SEM. Site-specific TEM samples from the interaction layer containing the terminal ends (e.g., U–7Mo and Al–Si alloys) were prepared with a FIB-INLO technique using a FEITM TEM200. A FEITM Tecnai F30 with a field emission source working at 300 keV was employed for the TEM analysis. The microstructure, composition, and phase constituents of samples were characterized using a variety of TEM techniques including bright/dark field imaging, high angle annular dark field (HAADF) via scanning TEM (STEM), X-ray energy dispersive spectroscopy (XEDS), selected-area and convergent beam electron diffraction (SAED and CBED). In this study, the HAADF imaging technique via STEM is valuable since the image intensity varies approximately proportional to the square of atomic number (Z^2). Phases with different composition exhibit different contrast on HAADF-STEM micrographs, analogous to backscatter electron imaging of SEM.

It should be noted that the interaction layer thickness is sensitive to the experimental conditions such as powder surface oxidation, interfacial contact conditions and gamma phase decomposition. This paper presents, to our best effort, results from typical representative interfacial regions, and the results indicate that the thickness of the interaction layer is quite uniform.

3. Results

Fig. 1 presents backscattered scanning electron micrographs from the four dispersion fuel plate samples examined in this study at a relatively low magnification to provide an overview of the fuel plates. A clear observation of typical interaction zones for the four samples is provided by backscattered electron micrographs presented in **Fig. 2**. The interaction layer that appears gray can be identified between the U–7Mo particles and Al–Si matrix. Consistently, samples with 5 wt.% of Si exhibited thicker and/or more continuous interaction layers than those with 2 wt.% Si before and after the anneal (i.e., “As2Si” vs. “As5Si” and “An2Si” vs. “An5Si”). The thickness of interaction layer is determined to be 90 ± 16 nm for sample “As2Si”, 660 ± 265 nm for sample “As5Si”, 394 ± 100 nm for sample “An2Si”, and 1239 ± 568 nm for sample “An5Si”.

Fig. 3 highlights the results from the TEM characterization of sample, as-fabricated with 2 wt.% Si, “As2Si”. The HAADF-STEM micrograph presented in **Fig. 3(a)** clearly shows the development of a very thin interaction layer between U–7Mo and Al–2Si. XEDS data acquired from the interaction layer (**Fig. 3(b)**) indicates a coexistence of U, Al, and Si. The appearance of Cu peak is due to the signal from the Cu TEM grid employed. The standard-less quantification of XEDS pattern gives a composition of $U_{58}Mo_2Al_{19}Si_{21}$ (at.%). Since the interaction layer is very thin (less than 100 nm) and surrounded by U–7Mo and Al–2Si matrix, the composition should be considered as semi-quantitative. Approximately 10 CBED patterns were acquired from random locations within the interaction layer to identify the constituent phases. Majority of the patterns acquired were identified to be $U_3Si_3Al_2$, and a representative, indexed TEM-CBED pattern is presented in **Fig. 3(c)**. A single CBED pattern (i.e., out of 10 acquired) from $U(Al,Si)_3$ phase was also obtained as presented in **Fig. 3(d)**. These results indicate that more than one phase has developed even at the very early stages of interaction. Both phases have very fine grains at nano-scale. The U–7Mo alloy was indexed as bcc- γ phase (pattern not shown) and no other U phase was observed. The space group, crystal structure, and lattice parameters of phases [35] relevant to this study are listed in **Table 5**.

Fig. 4 highlights the results from the TEM characterization of sample, as-fabricated with 5 wt.% Si, “As5Si”. Compared to the interaction layer of sample “As2Si” (with a thickness of 90 ± 16 nm), a thicker interaction zone (660 ± 265 nm) was observed in sample “As5Si” as seen in **Fig. 4(a)**. **Fig. 4(b)** presents a XEDS pattern acquired from the interaction area showing peaks of Si, Al, and U, corresponding to a composition of $U_{62}Mo_{0.1}Al_8Si_{30}$ (at.%). Among multiple electron diffraction patterns acquired and analyzed, only $U_3Si_3Al_2$ was identified. A typical TEM-CBED pattern is shown in **Fig. 4(c)**. The grain size of $U_3Si_3Al_2$ was very small in nano-

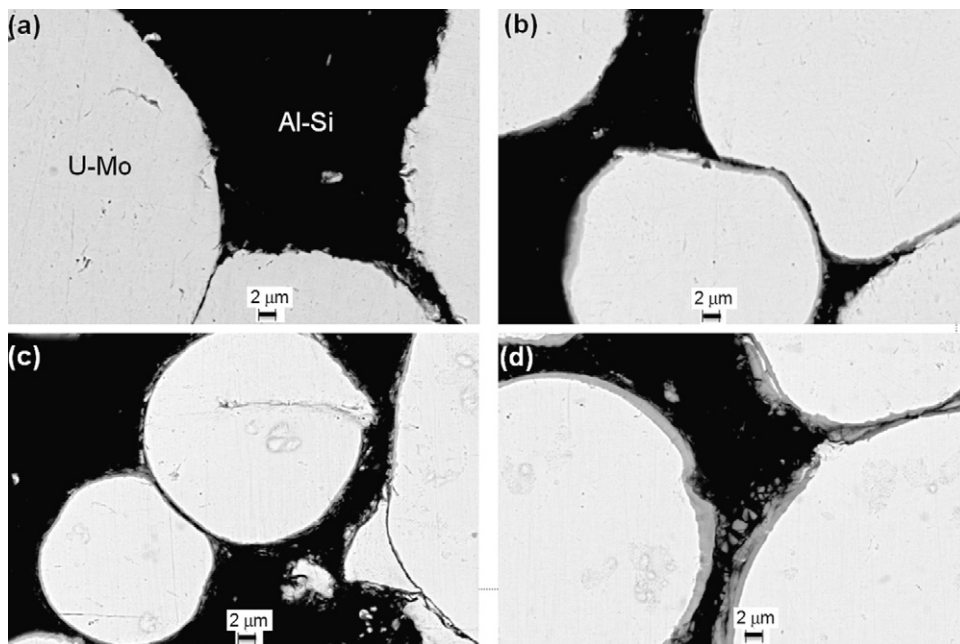


Fig. 2. Back-scattered SEM micrographs showing typical interaction zones between U(Mo) fuels and Al(Si) matrix in samples (a) "As2Si", (b) "As5Si", (c) "An2Si", and (d) "An5Si".

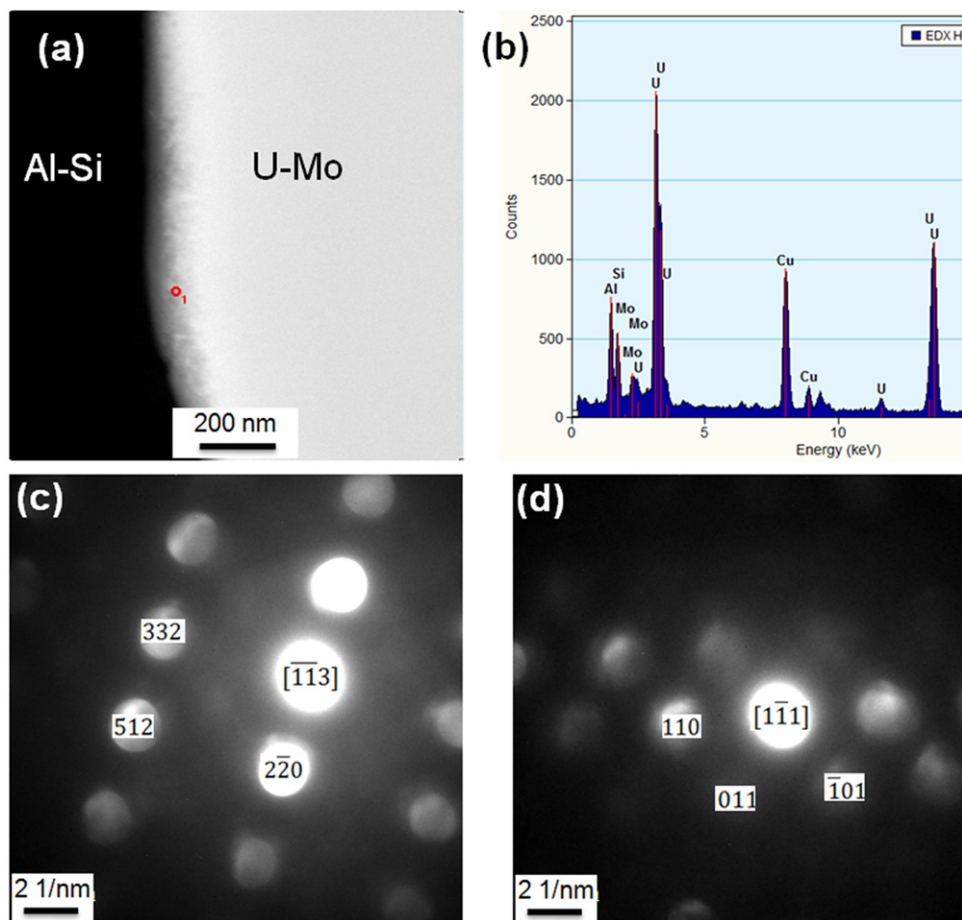


Fig. 3. TEM characterization results of sample "As2Si". (a) A HAADF-STEM micrograph showing interaction layer, (b) a typical XEDS pattern acquired from the interaction layer showing a coexistence of U, Al, and Si, (c) a representative TEM-CBED pattern of phase $U_3Si_3Al_2$ from the interaction layer, and (d) a TEM-CBED pattern of phase $U(Al, Si)_3$ from the interaction layer.

Table 5
Space group, crystal structure, and lattice parameters of relevant phases in the U(Mo)/Al(Si) fuel plates [35].

Phases	Space group (number)	Structure	Lattice parameters (Å)
U ₃ Si ₃ Al ₂	I4/mcm (140)	Tetragonal	7.628 × 10.799
U ₃ Si ₅	P6/mmm (191)	Hexagonal	4.028 × 3.852
U(Al, Si) ₃	Pm-3m (221)	Cubic	4.263
U(Al, Si) ₄	Imma (74)	Orthorhombic	4.41 × 6.27 × 13.71
U ₆ Mo ₄ Al ₄₃	P63/mcm (193)	Hexagonal	10.966 × 17.69
αU(Mo)	Cmcm (63)	Orthorhombic	2.8444 × 5.869 × 4.932
βU(Mo)	P42/mmm (136)	Tetragonal	10.759 × 5.656
γU(Mo)	Im-3m (229)	Cubic	3.534
U ₂ Mo	I4/mmm (139)	Tetragonal	3.427 × 9.834

scale, similar to that in sample “As2Si”. The U–7Mo alloy near the interface was indexed to be bcc-γ phase, and a typical SAED pattern is presented in Fig. 4(d).

The annealed samples with 2 and 5 wt.% Si, “An2Si” and “An5Si”, respectively, exhibited a significant evolution of constituent phases and microstructure, both in the interaction zone and in the U–7Mo particles. Figs. 5 and 6 highlight results from TEM characterization of samples “An2Si” and “An5Si”, respectively. An interaction zone, consisting of two layers, labeled as 1 and 2 in Fig. 5(a) for “An2Si” sample, was observed as presented in HAADF-STEM micrographs. XEDS data from layers 1 and 2, presented in Fig. 5(b) and (c), respectively, indicate that the layer 1 is enriched with Si (U₄₈Mo₃Al₄Si₄₅ in at.%) and the layer 2 is enriched with Al (U₃₁Mo_{0.1}Al₄₅Si₂₄ in at.%).

A closer examination with HAADF-STEM revealed that the Si-rich layer consists of multiple phases with different contrasts. Regions with a medium contrast in Si-rich layer (labeled as “A” in Fig. 5(a)) were identified to be U₃Si₅, and its CBED pattern is presented in Fig. 5(d). On the other hand, a few dark spots observed in Fig. 5(a) (labeled as “B”) correspond to the undesirable U₆Mo₄Al₄₃ phase whose CBED pattern is presented in Fig. 5(e). However, there is a very limited fraction of U₆Mo₄Al₄₃ phase in the Si rich layer. The Al-rich layer 2 in sample “An2Si” was amorphous with typical diffused diffraction patterns (not shown). Fig. 5(f) demonstrates the absence of diffraction contrast in bright-field micrograph. The formation of amorphous phase during diffusion reaction is not uncommon [36], and it is believed to be induced by a rapid interdiffusion at temperatures low enough to suppress nucleation of crystalline phases.

A much thicker two-layer interaction zone (more than 1 μm) was observed in sample “An5Si” as presented in Fig. 6(a). Similar to the “An2Si” specimen, the layer near to the U–Mo alloy was rich with Si (U₄₁Mo₃Al₁₄Si₄₂ in at.%), and the layer near the Al–Si alloy was Al-rich (U₃₆Mo₁Al₃₆Si₂₇ in at.%). Corresponding XEDS patterns from Si-rich and Al-rich layers are presented in Fig. 6(b) and (c), respectively. However, interface between these two layers was somewhat diffused as shown in Fig. 6(a). Both U₃Si₃Al₂ and U₃Si₅ phases were commonly identified in the Si-rich layer next to the U–Mo alloy, and their CBED patterns are presented in Fig. 6(d) and (e), respectively. The majority of the Al-rich layer (labeled as layer 2) was characterized to be U(Al, Si)₃ as shown by the CBED pattern in Fig. 6(f). However, this Al-rich layer contained some localized spots with variation in composition, as clearly evidenced by a com-

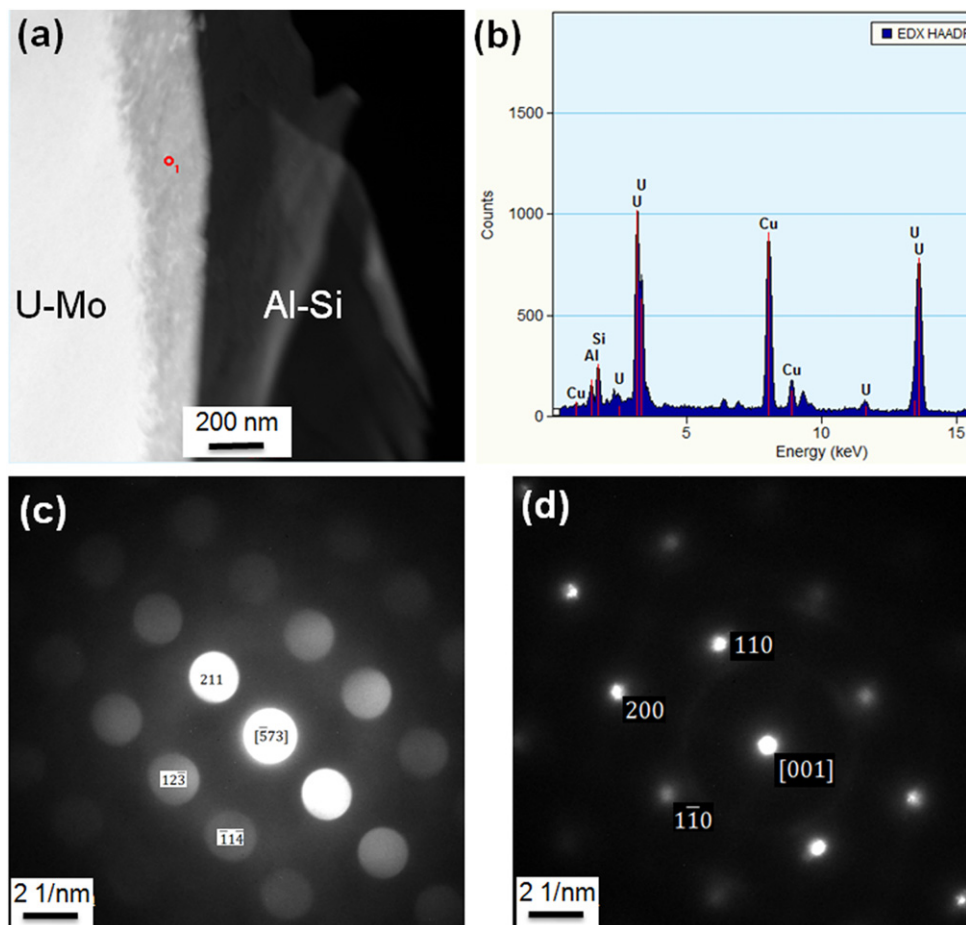


Fig. 4. TEM characterization results of sample “As5Si”. (a) A HAADF-STEM image showing a typical interaction layer, (b) a representative XEDS pattern from the interaction layer, (c) a TEM-CBED pattern of phase U₃Si₃Al₂ from the interaction layer, and (d) a TEM-SADP pattern of phase γU(Mo) from U(Mo) matrix.

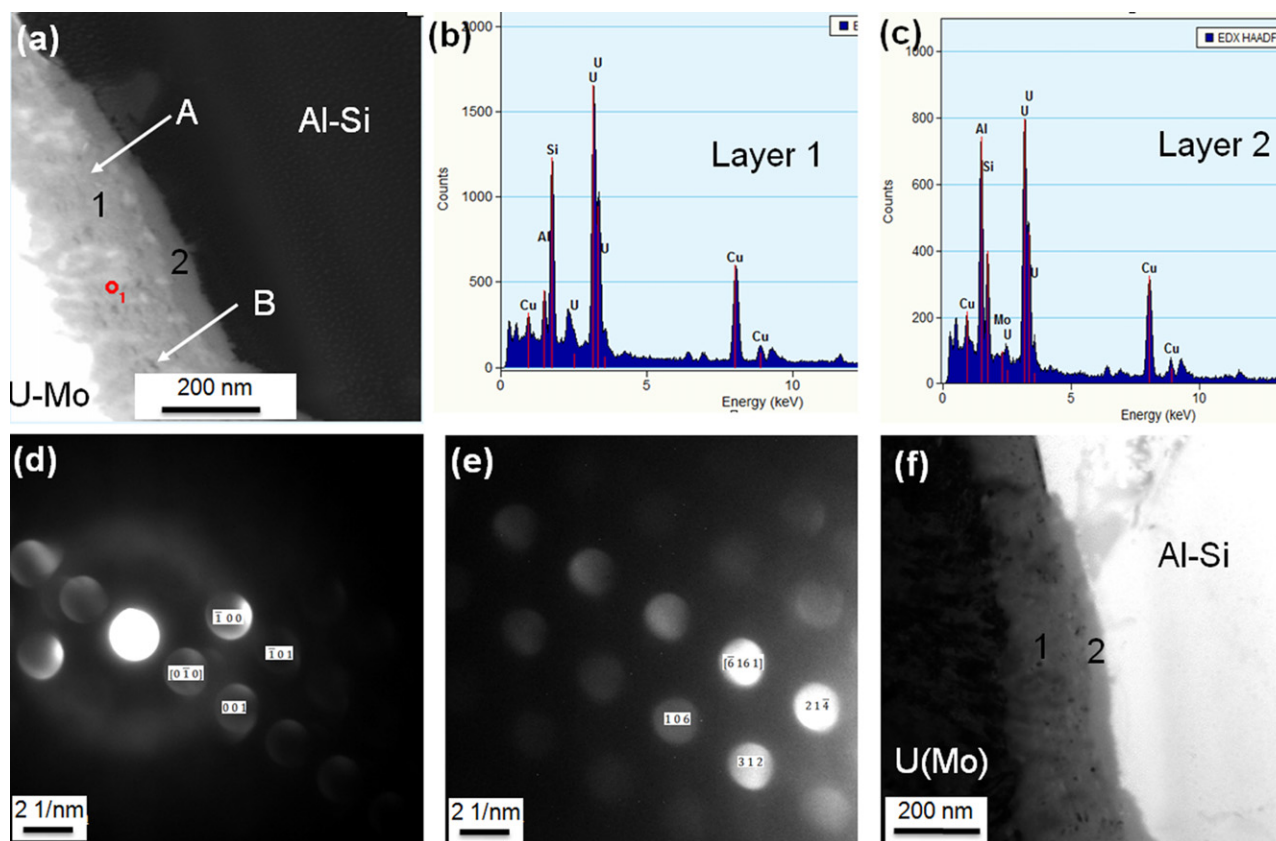


Fig. 5. TEM characterization results of sample “An2Si”. (a) A HAADF-STEM image showing a two-layer interaction zone (layer 1 and layer 2), (b) an XEDS spectrum from Si-rich layer (layer 1), (c) an XEDS pattern from Al-rich layer (layer 2), (d) a TEM-CBED pattern of phase U_3Si_5 from the medium-contrast in the Si-rich layer (labeled as “A” in (a)), (e) a TEM-CBED pattern of phase $U_6Mo_4Al_{43}$ from a few dark spots (labeled as “B” in (a)), and (f) a BF-TEM image showing an amorphous phase in Al-rich layer (layer 2) with an absence of any diffraction contrast.

plex HAADF-TEM contrast in Fig. 7(a). A few dark spots with high Al concentration and negligible Si content were observed in these regions as presented in Fig. 7(a) and (b). The composition was measured to be $U_{20}Mo_3Al_{75}Si_2$ (at.%). The TEM-CBED patterns acquired from these regions, presented in Fig. 7(c) and (d), were indexed to be $U(Al,Si)_4$ and $U_6Mo_4Al_{43}$, respectively.

A significant change in the microstructure and phase constituents was also observed in the U–7Mo alloy after the annealing at 475 °C for 4 h. Aforementioned, the as-fabricated U–7Mo alloys retained its γ -bcc structure with large grains. In contrast, Fig. 8(a) represents typical microstructure in the U–7Mo alloy from annealed samples, and shows the development of small grains with multiple phases including α -U(Mo), β -U(Mo), γ -U(Mo), and δ - U_2Mo . The TEM-CBED patterns acquired from these phases are presented in Fig. 8(b) through (e), respectively.

4. Discussion

4.1. Effect of Si content on the thickness of initial interaction layers

In this investigation where initial formation and evolution of very thin (typically less than 1 μm) interaction layer were examined, thicker interaction layers formed in samples with a higher concentration of Si in Al(Si) matrix have been consistently observed. This result does not agree with previous investigations that typically employed solid-to-solid diffusion couples [37] annealed isothermally for a long time to obtain relatively thick (e.g., hundreds of micrometers) interaction layer, where the addition of Si in the Al alloy matrix significantly reduced the growth rate of

interaction layers. The thickness growth of interaction layers can be controlled by the interfacial reaction to form the product or the diffusion of Si from Al(Si) matrix to the interaction zone. In case of reaction-controlled growth, however, similar interaction layer thickness in controlled samples (“As2Si” vs. “As5Si”, “An2Si” vs. “An5Si”) should be expected since they experienced the same processing conditions (e.g., fabrication temperature and time) and the reaction rate is expected to be similar to each other. Note that this statement is based on the fact that the controlled samples examined in this study consist of similar phases and composition in the interaction layer. In the diffusion couple study (e.g., the one by Allenou et al. [28]), situation can be totally different. It was found that different Si concentration yields totally different layers and phases. In this study, a significant variance of the product layer thickness suggests that the diffusion of Si controls the growth of interaction layers. The solid solubility of Si in Al matrix is very limited (less than 1 at.% at 400 °C) [38]. Consequently, an increase of Si from 2 wt.% to 5 wt.% in Al(Si) matrix does not lead to a significant increase of chemical potential of Si. However, a higher concentration of Si may more resourcefully reduce the thickness of Si-depleted region in the Al matrix near the interaction layer [16,17,20,21,23], which may consequently result in a thicker interaction layer.

4.2. Initial evolution of thin interaction layers of as-fabricated and annealed fuel plates

A clear understanding of the phase formation and its evolution in the interaction layer is important in predicting its behavior under irradiation. In both as-fabricated U(Mo)/Al(Si) samples (“AS2Si” and “AS5Si”), a single layer, mainly composed of $U_3Si_3Al_2$ has been iden-

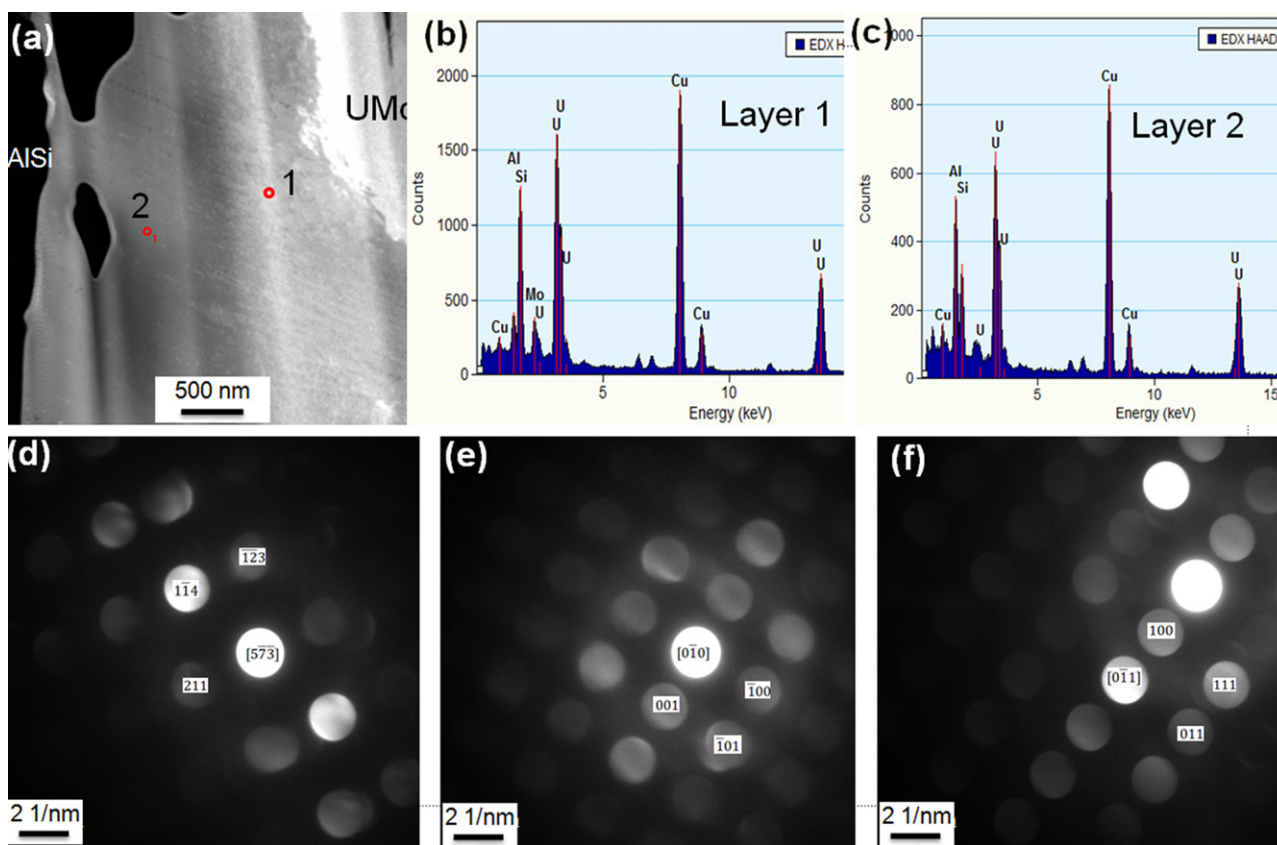


Fig. 6. TEM characterization results of sample “An5Si”. (a) A HAADF-STEM image showing a two-layer interaction zone (layer 1 and layer 2), (b) an XEDS spectrum from Si rich layer (layer 1), (c) an XEDS spectrum from Al-rich layer (layer 2), (d) a representative indexed TEM-CBED pattern of phase $U_3Si_3Al_2$ from Si-rich layer (layer 1), (e) a typical TEM-CBED pattern of phase U_3Si_5 from Si-rich layer (layer 1), and (f) a TEM-CBED pattern of phase $U(Al, Si)_3$ from Al rich layer (layer 2).

tified. Based on the Effective Heat of Formation (EHF) model [39], the phase formed at the interface is influenced by both the heat of formation of candidate phases and the effective composition at the interface. The coexistence of U, Si, and Al at the interface between U(Mo) and Al(Si) may make the nucleation of $U_3Si_3Al_2$ favorable. The appearance of $U_3Si_3Al_2$ phase in the interaction layer was first reported in our recent FIB/TEM studies on U(Mo)/Al(Si) fuel plates [31,32], typically in samples with very thin “initial” interaction layers. Most studies based on XRD and SEM/XEDS characterization of thick interaction layers [18–29], however, did not identify this phase, which suggests that $U_3Si_3Al_2$ may not be stable upon further annealing.

The phase evolution of samples annealed at 475 °C is likely to be influenced by local Si concentration. Suggested by atomistic modeling [15–17] and experimental observations [20,21,23], U has a larger affinity for Si than for Al, and Si is accumulated in the interaction zone near the U(Mo) particle. Due to the accumulation of Si in the interaction zone, a Si-depleted region has been commonly observed in the Al(Si) matrix near the product layer [20,21,23]. It is therefore expected that the initial $U_3Si_3Al_2$ product layer has two distinct interfaces: the one near the U–Mo side having an accumulated high concentration of Si, while the other near the Al(Si) side containing depleted Si. A high Si concentration at the U(Mo)/ $U_3Si_3Al_2$ interface drives the nucleation of U–Si phases, such as U_3Si_5 and $U(Si,Al)_3$, at the expense of $U_3Si_3Al_2$, U(Mo) and Si. On the other hand, the deficiency of Si at the $U_3Si_3Al_2$ /Al(Si) interface may produce the U–Al phases, such as $U(Al, Si)_3$. The phase formation of $U(Al, Si)_4$ and $U_6Mo_4Al_{43}$ in sample “An5Si” (Fig. 7) further confirms such an explanation. As shown in Fig. 7, these two phases were observed typically far away from the Si-rich layers, and a negligible Si concentration ($U_{20}Mo_3Al_{75}Si_2$ in at.%) was identified

from their XEDS data. It is reported that the appearance of these two phases is related to the local concentration of Si, and a low Si concentration cannot effectively inhibit their formation [19–21]. The formation of $U_6Mo_4Al_{43}$ in the Si-rich layer of sample “An2Si” (Fig. 5), however, is believed to be induced by local composition variation.

4.3. Influence of Si observed as a function of interaction layer thickness

This study presented the initial formation and evolution of very thin (typically less than 1 μm) interaction layer in the fuel plates. It should be noted that the influence of Si content on the phase formation and growth may be complex as the interaction layer grows with time. Allenou et al. [28] examined solid-to-solid diffusion couples consisting of U–7 wt.% Mo vs. Al–Si alloy with varying Si concentration of 2, 5, 7, and 10 wt.%, annealed at 450 °C for 2 h. The interaction layer grew up to 100 μm , and the rate of growth varied as a function of Si content. An increase in Si-content, up to 5 wt.%, decreased the thickness of the interaction layer, and did not influence the rate of growth with further increase in Si-content (e.g., 7 and 10 wt.%) [28]. Similar trend has been reported by Perez et al. [37], who also examined solid-to-solid diffusion couples with relatively thick interaction layers.

In a typical diffusion couple study with longer anneal time, an increase in Si content up to a few wt.% decreases the growth rate of the interaction layer since diffusional flux necessary to maintain the slow-growing U–Si compound [8] is more sufficient. This sufficiency is due to (1) an increased chemical potential of Si in Al solid solution, and (2) unlimited reservoir of Si in infinite boundary condition for solid-to-solid diffusion couples. Another

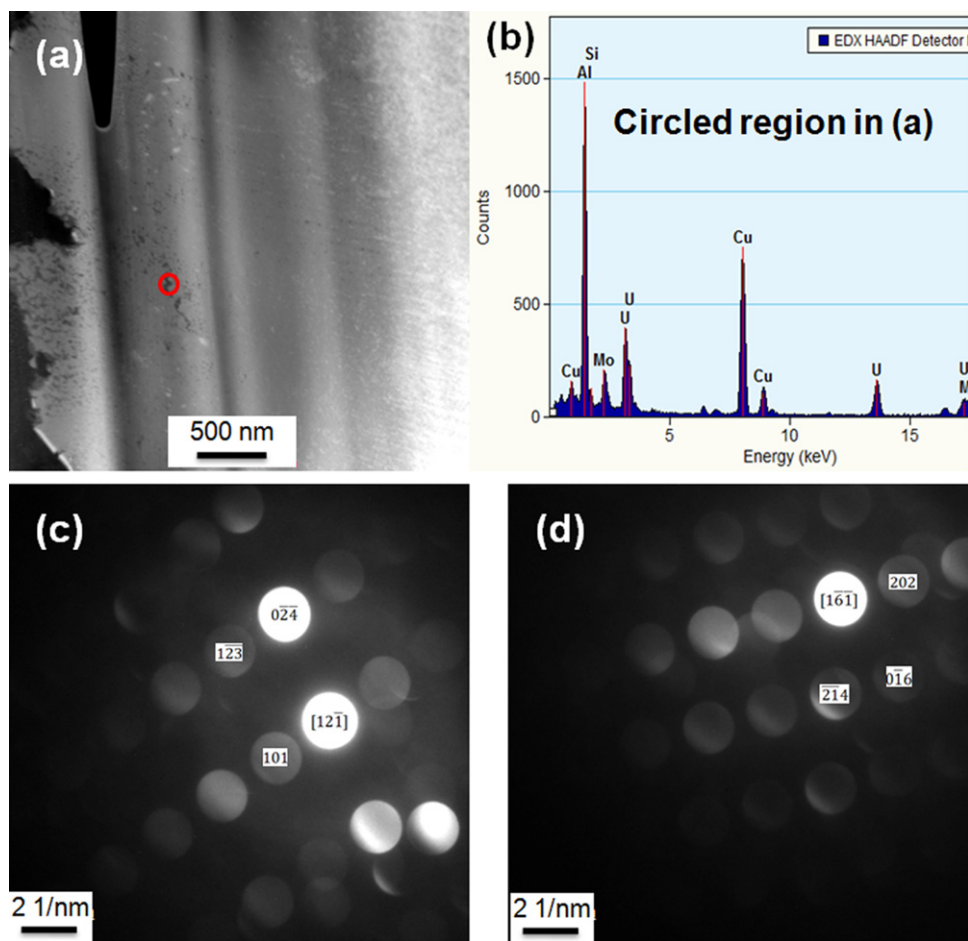


Fig. 7. Further TEM characterization results of Al rich interaction layer near Al(Si) matrix of sample “An5Si”. (a) A HAADF-STEM micrograph showing a complex contrast in the Al rich interaction layer near Al(Si) matrix, (b) a XEDS pattern acquired from the circled dark region (a) showing a high concentration of Al and negligible Si, (c) $U(\text{Al}, \text{Si})_4$ and (d) $U_6\text{Mo}_4\text{Al}_{43}$ identified from patterns acquired from the circled dark regions in Al rich layer showing in (a).

factor that can contribute is an increase in diffusion coefficient (e.g., mobility) with higher Si content. When the Si-content is higher than 5 wt.%, for example, above the solubility limit of Al solid solution, the chemical potential of Si in Al solid solution remains the same in the two-phase Al–Si alloy. Of course, the unlimited reservoir of Si also remains the same.

In the studies with diffusion couples [28,37], separation of Si- and Al-rich regions within the interaction layers are typically reported. Furthermore, many different phases were identified. For example, in the diffusion-couple study by Allenou et al. [28], the Si rich layer (near to the Al matrix side) was identified to be $U(\text{Al}, \text{Si})_3$ and $U\text{Mo}_2\text{Al}_{20}$, while the Al rich layer (near to the U–Mo side) contains $U\text{Al}_3$ and $U_6\text{Mo}_4\text{Al}_{43}$ for diffusion couples with Si content less than 5 wt.% in the Al–Si alloy. For diffusion couples with more than 5 wt.% alloying addition of Si in Al, the Si rich layer (near to the U–Mo side) contains $U_3(\text{Si}, \text{Al})_5$ and $U(\text{Al}, \text{Si})_3$, while the Al rich layer (near to the Al side) was indexed to be $U(\text{Al}, \text{Si})_3$ and $U\text{Mo}_2\text{Al}_{20}$.

In this TEM study to examine the initial growth of interaction layer (thickness typically less than 1 μm), the growth rate of interaction layer, at least initially, increased with increasing Si concentration. Also during this initial stage, the Si-rich layer appeared on the U–Mo side, while the Al-rich layer appeared on the Al–Si matrix side. Furthermore, the phase constituents of each layer were different. The “as-fabricated” interaction layer mainly composed of single phase, $U_3\text{Al}_3\text{Si}_2$, while the two layers in the annealed samples consisted of $U_3\text{Si}_5$ and $U_3\text{Si}_3\text{Al}_2$ in the Si-rich layer and $U(\text{Al}, \text{Si})_3$, $U(\text{Al}, \text{Si})_4$, $U_6\text{Mo}_4\text{Al}_{43}$ and amorphous phase in the Al-rich layer.

These differences in observations are typical for different diffusion couple studies [28,40,41] and “thin” interaction layer studies [30–32]. Based on this study, the evolution of a single phase $U_3\text{Si}_3\text{Al}_2$ -layer in the as-fabricated sample into two layers (Si-rich and Al-rich) in annealed samples is clear. Upon further growth, analogous to diffusion couples, the phases present in initial interaction layer may or may not be stable, depending upon the diffusional flux of Si that would significantly vary since this is not a solid-to-solid diffusion couple study with infinite boundary condition. Results from this study, particularly after the anneal should be strongly influenced by local chemical potential of Si in Al solid solution and “locally-limited Si-reservoir.”

4.4. Amorphous phase and other products in interaction layer

Failure of post-irradiation fuels has been linked frequently to the presence of an amorphous phase in the interaction layer between U–Mo and Al–Si [4]. The reason for the failure has been attributed to the formation of fission bubbles during irradiation [9]. The glassy layer cannot support the bubble lattice, and consequently causes the bubbles to coalesce and lead to the development of large voids. For samples without the irradiation damage, the formation of amorphous phase during diffusion reaction is commonly believed to be induced by a rapid interdiffusion at relatively low temperatures where the nucleation of crystalline phases is suppressed. Because of irradiation enhanced atomic mobility and interdiffusion, the formation of amorphous phase would be easier, and this may be

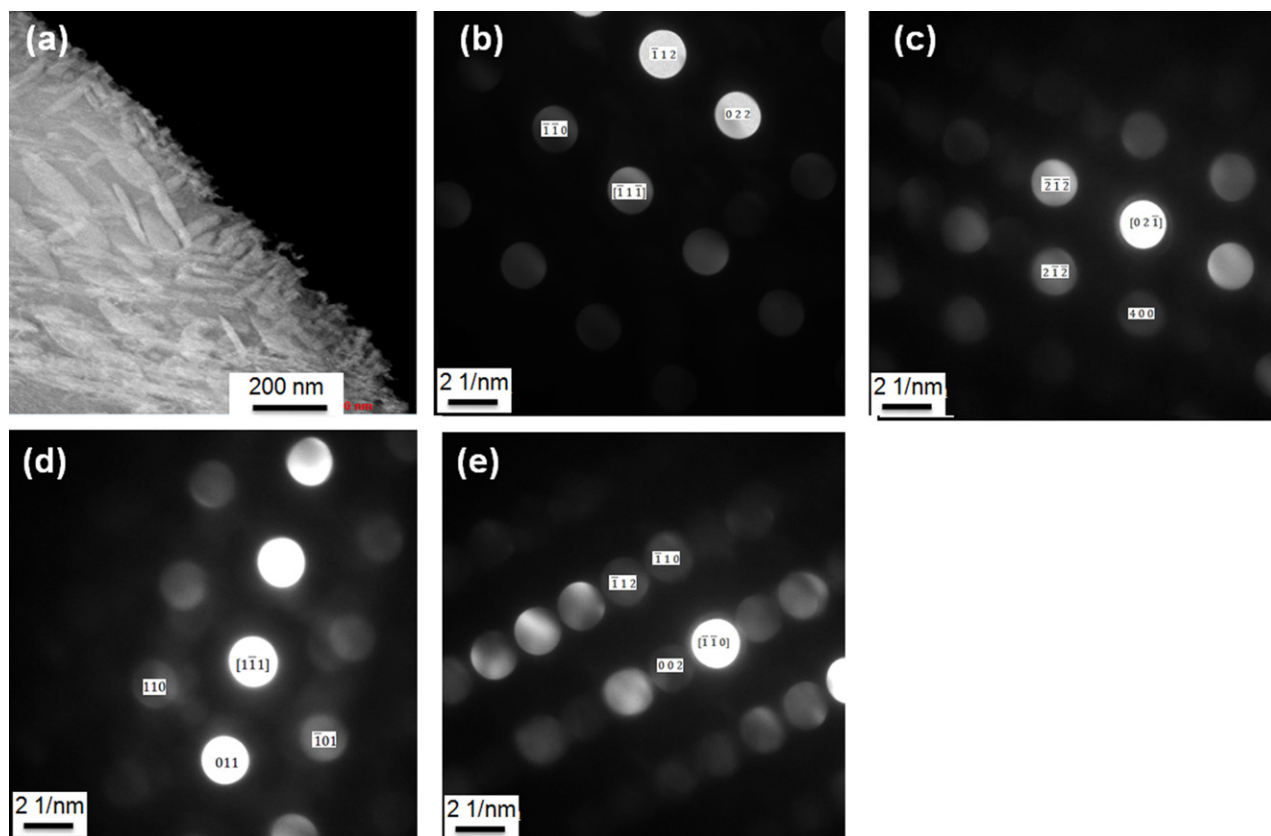


Fig. 8. (a) TEM images showing U(Mo) microstructure in annealed sample “An2Si”. Phases including (b) α U(Mo), (c) β U(Mo), (d) γ U(Mo) and (e) U_2Mo have been identified. Similar microstructure and phases also appeared in sample “An5Si”.

the reason for commonly reported irradiation-induced amorphous phase in interaction layer of U–Mo/Al–Si dispersion fuel.

In this study, for the first time, we identified the formation of amorphous phase in the interaction layer prior to irradiation of U–Mo/Al–Si dispersion fuel. There are two potential reasons why the amorphous phase was observed in this study. First, the sample was annealed at relatively low temperature (475 °C), which may be enough for the U–Mo/Al–Si interdiffusion, but not enough to nucleate new crystalline phases. Second, this amorphous phase is very thin, and can limit the total number of potential nuclei. It is still not clear if this amorphous layer is stable with further annealing and/or under irradiation. Amorphous phase can be characterized by its composition and corresponding microstructure (e.g., nearest atom distance). The composition of the amorphous layer observed in this study ($U_{31}Mo_{0.1}Al_{45}Si_{24}$ in at.%) is different from that commonly found in interaction layer (i.e., 80 at.% Al).

4.5. Remarks on irradiation behavior

Irradiation performance of the interaction layer can be correlated with the structure and phase development of dispersion fuel after manufacturing. The formation of Si-rich layer around the U–Mo/Al–Si dispersion fuel is important to the irradiation performance. One potential beneficial role of Si-rich layer is the prevention of rapid reaction that produces Al-rich compounds that grow rapidly and are not stable under irradiation. The Si-rich phases such as $U_3Al_3Si_2$, U_3Si_5 , $U(Si,Al)_3$, and USi_2 were observed in this study. The appearance of specific phases may depend on the Si content (i.e., local and overall) and heat treatment.

Unfortunately, the Si-rich layer may evolve into other phases during growth upon further annealing and/or under irradiation. As discussed, the Si-rich layer in initial interaction layer of dispersion

fuels with 2 wt.% Si may completely evolve into other U–Al compounds upon further growth due to insufficient Si diffusional flux (e.g., local and/or overall chemical potential of Si). Therefore it may be beneficial to increase Si concentration so that chemical potential that drives the diffusion remains high and its local variation is minimized.

Another factor important to the performance of dispersion fuels is the formation of undesirable U–Al compounds (e.g., UAl_4 and $U_6Mo_4Al_{43}$) in Al-rich layer due to the formation of Si-depleted region. In this study of initial layer formation, small amounts of these phases appeared even when the Si-rich layer was dominant. If the formation of UAl_4 and $U_6Mo_4Al_{43}$ phases can be suppressed locally and globally by adding Si in Al alloy, a higher Si concentration may also be helpful to minimize the fraction of these undesirable phases.

5. Conclusions

A detailed characterization of as-fabricated and 475 °C annealed U–7 wt.% Mo dispersion fuel in Al–Si matrix plates, namely, “As2Si”, “As5Si”, “An2Si”, and “An5Si” has been carried out. Fuel plates with a 5 wt.% of Si consistently produced thicker interaction layers between U(Mo) particles and Al(Si) matrix, than those with 2 wt.% Si, when processed under the same conditions. A single layer of interaction zone was observed for as-fabricated samples (i.e., “As2Si”, “As5Si”), and this layer was identified mainly to be the $U_3Si_3Al_2$ phase. The annealed samples contained a two-layered interaction zone: a Si-rich layer near the U–Mo side, and an Al-rich layer near the Al–Si matrix side. U_3Si_5 appeared as the main phase in the Si rich layer in sample “An2Si”, while both U_3Si_5 and $U_3Si_3Al_2$ were identified in sample “An5Si”. The Al-rich layer in sample “An2Si” was amorphous, whereas that in sample “An5Si”

was mostly crystalline $U(Al,Si)_3$, along with a very small fraction of $U(Al,Si)_4$ and $U_6Mo_4Al_{43}$ near the Al–Si matrix.

Acknowledgements

This work was supported by the U.S. Department of Energy, Office of Nuclear Materials Threat Reduction (NA-212), National Nuclear Security Administration, under DOE-NE Idaho Operations Office Contract DE-AC07-05ID14517. Accordingly, the U.S. Government retains a non-exclusive, royalty-free license to publish or reproduce the published form of this contribution, or allow others to do so, for U.S. Government purposes.

References

- [1] J.L. Snelgrove, G.L. Hofman, M.K. Meyer, C.L. Trybus, T.C. Wiencek, Nuclear Engineering and Design 178 (1997) 119–126.
- [2] M.K. Meyer, G.L. Hofman, S.L. Hayes, C.R. Clark, T.C. Wiencek, J.L. Snelgrove, R.V. Strain, K.H. Kim, Journal of Nuclear Materials 304 (2002) 221–236.
- [3] K.H. Kim, J.M. Park, C.K. Kim, G.L. Hofman, M.K. Meyer, Nuclear Engineering and Design 211 (2002) 229–235.
- [4] A. Leenaers, S. Van den Berghe, E. Koonen, C. Jarousse, F. Huet, M. Trotabas, M. Boyard, S. Guillot, L. Sannen, M. Verwerft, Journal of Nuclear Materials 335 (2004) 39–47.
- [5] G.L. Hofman, M.R. Finlay, Y.S. Kim, Proceedings of International Meeting on PERTR, Vienna, Austria, November 7–12, 2004.
- [6] S. Van den Berghe, W. Van Renterghem, A. Leenaers, Proceedings of the XXIX PERTR International Meeting, Prague, Czech Republic, 23–27th September, 2007.
- [7] F. Mazaudier, C. Proye, F. Hodaj, Journal of Nuclear Materials 377 (2008) 476–485.
- [8] E. Perez, D.D. Keiser, Y.H. Sohn, Phase constituents and microstructure of inter-action layer formed in U–Mo alloys vs. Al diffusion couples annealed at 873 K, Metallurgical and Materials Transactions, doi:10.1007/s11661-011-0733-9.
- [9] S. Van den Berghe, W. Van Renterghem, A. Leenaers, Journal of Nuclear Materials 375 (April (3)) (2008) 340–346.
- [10] Good Practices for Qualification of High Density Low Enriched Uranium Research Reactor Fuels, IAEA Nuclear Energy Series, No. NF-T-5.2. International Atomic Energy Agency.
- [11] D.D. Keiser, A.B. Robinson, J.F. Jue, P. Medvedev, D.M. Wachs, M.R. Finlay, Journal of Nuclear Materials 393 (2009) 311–320.
- [12] G. Hofman, Y. Kim, H. Ryu, M. Finlay, Proceedings of RERTR 2006, Cape Town, Republic of South Africa, October 29–November 2, 2006.
- [13] S.K. Yeon, J.R. Ho, G.L. Hofman, S.L. Hayes, M.R. Finlay, D.M. Wachs, G.S. Chang, Proceedings of RERTR 2006, Cape Town, Republic of South Africa, October 29–November 2, 2006.
- [14] M. Ripert, S. Dubois, P. Boulcourt, S. Naury, P. Lemoine, Proceedings of RRFM 2006, Sofia, Bulgaria, April 30–May 3, 2006.
- [15] J. Garces, G. Bozzolo, G. Hofman, J. Rest, Proceedings of the 27th International Meeting on Reduced Enrichment for Research and Test Reactors, Boston, USA, November 6–10, 2005.
- [16] J.E. Garces, G. Bozzolo, G. Hofman, J. Rest, Applied Physics Letters 90 (2007), 074104/1-074104/3.
- [17] J.E. Garces, G. Bozzolo, G. Hofman, J. Rest, Computational Materials Science 40 (2007) 6–19.
- [18] M. Cornen, X. Iltis, F. Mazaudier, S. Dubois, P. Lemoine, Materials Research Society Symposium Proceedings 1043E (2008) Paper #: 1043-T09-10.
- [19] R. Boucher, E.D. Alliages, Journal of Nuclear Materials 1 (1959) 13–27.
- [20] L.S. DeLuca, H.T. Sumsion, Proceedings of KAPL 1747, MA, 1957.
- [21] D. Kramer, Journal of Nuclear Materials 4 (1961) 281–286.
- [22] M. Cornen, F. Mazaudier, X. Iltis, M. Rodier, S. Dubois, P. Lemoine, Proceedings of RRFM 2007, Lyon, France, March 11–15, 2007.
- [23] Y. Kim, Proceeding of RERTR 2005, Boston, USA, November 6–10, 2005.
- [24] A. Savchenko, A. Vatulin, I. Dobrikova, Y. Kononov, Proceedings of RRFM 2006, Sofia, Bulgaria, April 30–May 3, 2006.
- [25] M. Mirandou, S. Balart, C. Varela, S. Arico, A. Fortis, Proceedings of RERTR 2007, Prague, Czech Republic, September 23–27, 2007.
- [26] M.I. Mirandou, S.F. Arico, S.N. Balart, L.M. Gribaudo, Materials Characterization 60 (2009) 888–893.
- [27] M. Mirandou, S. Arico, M. Rosenbusch, M. Ortiz, S. Balart, L. Gribaudo, Journal of Nuclear Materials 384 (2009) 268–273.
- [28] J. Allenou, H. Palancher, X. Iltis, M. Cornen, O. Tougait, R. Tucoulou, E. Welcomme, P. Martin, C. Valot, F. Charollais, M.C. Anselmet, P. Lemoine, Journal of Nuclear Materials 399 (2010) 189–199.
- [29] J.M. Park, H.J. Ryu, S.J. Oh, D.B. Lee, C.K. Kim, Y.S. Kim, G.L. Hofman, Journal of Nuclear Materials 374 (2008) 422–430.
- [30] D.D. Keiser, Diffusion and Defect Data—Solid State Data, Pt. A: Defect and Diffusion Forum 266 (2007) 131–148.
- [31] D.D. Keiser, Jr., B. Yao, E. Perez and Y.H. Sohn, Proceedings of the 31st International Meeting on Reduced Enrichment for Research and Test Reactors (RERTR 2009), Beijing, China, November 1–5, 2009, INL/CON-09-17107.
- [32] D.D. Keiser, J.F. Jue, B. Yao, E. Perez, Y.H. Sohn, C.R. Clark, Journal of Nuclear Materials 412 (1) (2011) 90–99.
- [33] J. Gan, D. Keiser, D. Wachs, B. Miller, T. Allen, M. Kirk, J. Rest, Journal of Nuclear Materials 407 (2010) 48–54.
- [34] X. Iltis, F. Charollais, M. Anselmet, P. Lemoine, A. Leenaers, S. Van den Berghe, E. Koonen, C. Jarousse, D. Geslin, F.H. Frery, Proceeding of RERTR-2010 Meeting, Lisbon, Portugal, October 10–14, 2010.
- [35] The Inorganic Crystal Structure Database (ICSD), FIZ Karlsruhe, 2004.
- [36] K.N. Tu, Annual Review of Materials Science 15 (1985) 147–176.
- [37] E. Perez, D.D. Keiser Jr., Y.H. Sohn, Proceedings of the 31st International Meeting on Reduced Enrichment for Research and Test Reactors (RERTR 2009), Beijing, China, November 1–5, 2009, INL/CON-09-17105.
- [38] T.B. Massalski, H. Okamoto, Binary Alloy Phase Diagrams, ASM International, Ohio, 1990.
- [39] R. Pretorius, C.C. Theron, A. Vantomme, J.W. Mayer, Critical Reviews in Solid State and Materials Sciences 24 (1999) 1–62.
- [40] M. Cornen, M. Rodier, X. Iltis, S. Dubois, P. Lemoine, Proceedings of the 2008 RRFM ENS Meeting, Hamburg, Germany, March 25, 2008.
- [41] M. Cornen, X. Iltis, F. Mazaudier, S. Dubois, P. Lemoine, Proceedings of the 2007 MRS Fall Meeting, Boston, USA, November 27–29, 2007.